Postprint of: Derkacz P., Musznicki P., Chrzan P., EMI attenuation in a DC-DC buck converter using GaN HEMT, IEEE JOURNAL OF EMERGING AND SELECTED TOPICS IN POWER ELECTRONICS (2020), Vol. 9, No 4, pp. 4146 - 4152,

DOI: 10.1109/JESTPE.2020.2987638

EMI attenuation in a DC-DC buck converter using GaN HEMT

Pawel B. Derkacz , *Student Member, IEEE,* Piotr Musznicki , and Piotr J. Chrzan , *Senior Member, IEEE*

***Abstract*—A dc-dc buck converter using gallium nitride (GaN) high electron mobility transistors (HEMT) is experimentally investigated at the discontinuous current mode (DCM) and at the triangular current mode (TCM) operation. The paper objective is to specify the power conversion efficiency and attenuation of common mode (CM) and differential mode (DM) noise voltage, measured at the line impedance stabilization network (LISN) for compared control strategies. Zero voltage switching achieved for the TCM operation improves efficiency with reference to the DCM operation. However, significant attenuation of electromagnetic interference (EMI) spectra is obtained for TCM operation with capacitive snubber. Sizing of capacitor snubber dependent on parasitic inductances of commutation circuit and rapid switching of GaN HEMTs are illustrated.**

***Index Terms*—Buck converter, triangular current mode (TCM), zero voltage switching (ZVS), electromagnetic interference (EMI), gallium nitride high electron mobility transistor (GaN HEMT)**

I. Introduction

EXTENSIVE development of wide-band gallium nitride (GaN) power transistors reveals new horizons in converter design achieving increased operation frequency, higher power density, lower switching and conduction losses [1], [2]. Particularly, superiority of the GaN high electron mobility transistor (HEMT) in cascode structure over silicon MOSFET and IGBT technologies has been proved in a number of comparative research tests carried out for buck-boost dc-dc converters [3] or inverter configurations [4], [5]. I n order to properly exploit high frequency switching ability of GaN HEMT devices, the design objective of an ultralow inductance commutation cell (including package and circuit layout) should be fulfilled [6]–[9].

In high frequency dc-dc buck-boost converters, for limitation of turn on switching losses, the zero voltage switching (ZVS) conditions are strongly recommended. The ZVS operation may be directly achieved in a resonant circuit consisting of the filter i nductor a nd t he s witches c apacitance. B y applying control of the triangular current mode (TCM) [10] (defined also, as critical current mode [11]), resonant transitions are evoked at successive converter state commutations. Relatively large triangular current waveform ripples characterizing TCM operation can be attenuated by introducing interleaved multiphase topology [12], in a form of coupled inductors [11] or using circuit extension with additional clamp switch [13]. However, an impact of high frequency dv/dt switching on electromagnetic interference (EMI) emission has not been specifically considered in above works. The EMI effects including near field couplings, signal stability, layout, operation mode and passive components are presented in [14]. The impact of parasitic capacitance between PCB board and heatsink is described in [15]. The modelling of CM impedance is performed to predict the conducted EMI in [16], [17].

In view of the growing demand for application of GaN HEMT technology, in this paper, EMI conducted emission of a dc-dc buck converter operation in the TCM ZVS was investigated and compared with the conventional hard switching discontinuous current mode (DCM) control technique. Experimental setup, as in Fig. 1, consisted of GaN HEMT based dc-dc buck converter with resistive load, supplied by the line stabilization network (LISN) from the dc voltage source. The paper objective is to specify the power conversion efficiency and attenuation of common mode (CM) and differential mode (DM) noise voltage of the compared switching control strategies. For the TCM operation, the sizing of an additional snubber capacitor is considered to reduce the switch turn off voltage overshoot and to stabilize resonant transition period. In section II, the switching strategies are briefly introduced. In section III, the test setup, implemented control strategies with energy based analysis of snubber capacitor are presented. Next, experimental results of EMI and converter efficiency measurements are compared, that are resumed in conclusions.

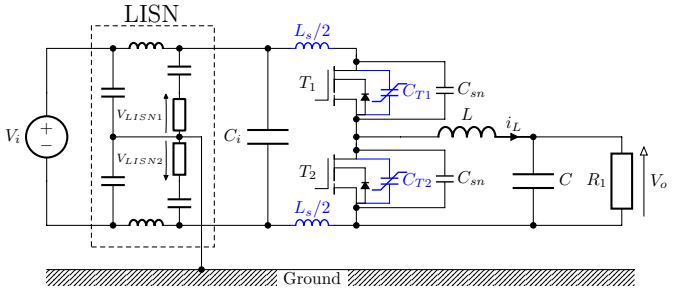

Fig. 1. Test circuit of GaN HEMT buck converter

This article has been accepted for publication in a future issue of this journal, but has not been fully edited. Content may change prior to final publication. Citation information: DOI 10.1109/JESTPE.2020.2987638, IEEE Journal of Emerging and Selected Topics in Power Electronics

II. Switching strategies

A. DCM strategy

For the purpose of comparative study, the DCM waveforms are recalled in Fig. 2. with corresponding operation modes presented in Fig. 3. During the interval $[t_0 : t_1]$ when the T_1 is on, the inductor current i_L increases linearly. At instant t_1, the T_1 turns off. Voltage v_{T1} is rising and capacitance C_{T1} changes from a large to low value according to the nonlinear capacitance characteristic. This involves providing a charge to C_{T1} and discharge of C_{T2}. After T_1 is turned off $[t_2 : t_3]$, the inductor current i_L decreases linearly flowing through the load and the body diode of transistor T_2.

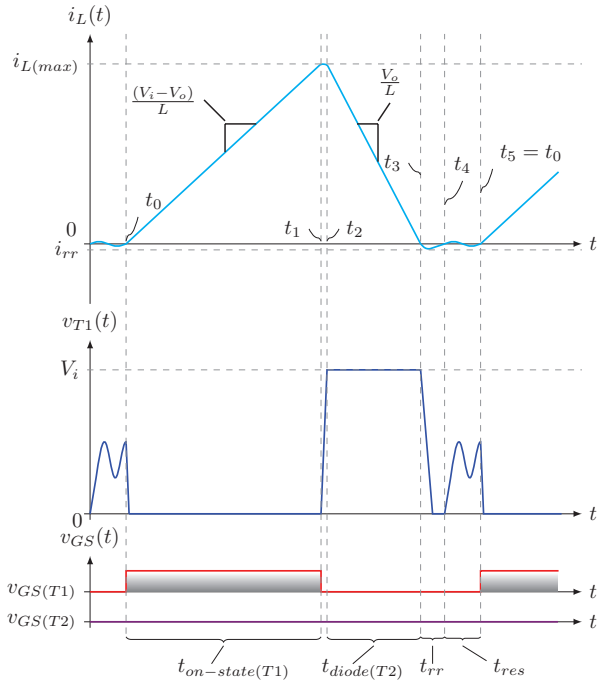

Fig. 2. DCM waveforms

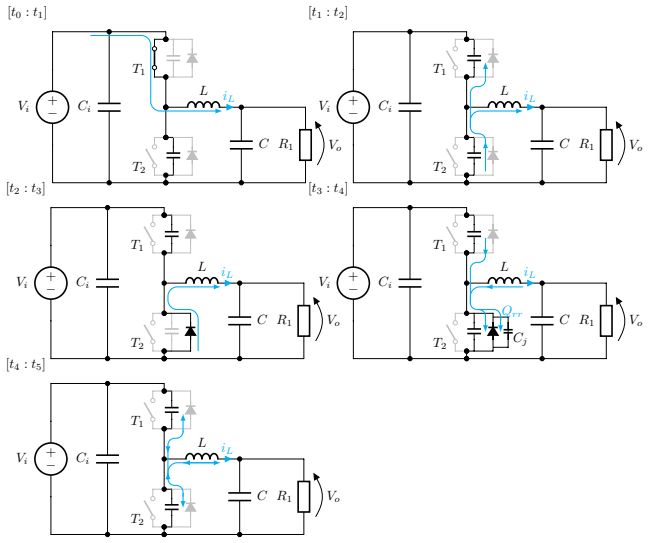

Fig. 3. DCM operation subcircuits

When i_L reaches zero, the reverse recovery charge Q_{rr} has to be provided to turn off the body diode – exciting oscillatory currents from capacitances: C and C_{T1}. In the interval $[t_4 : t_5]$ the C_{T1} and C_{T2} are reloading in resonant circuit with the inductor L causing voltage oscillations across transistors until next period begins [18].

B. TCM strategy

Similarly to the preceding case, the TCM waveforms are presented with operation modes respectively in Fig. 4. and Fig. 5.

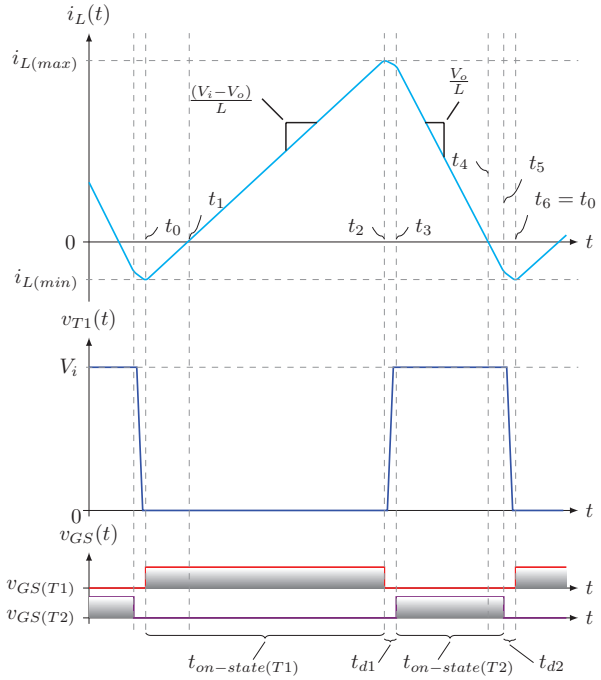

Fig. 4. TCM waveform

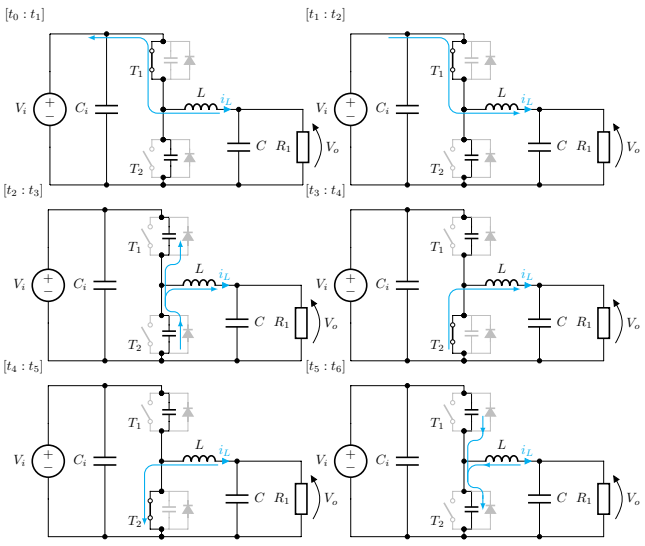

Fig. 5. TCM operation subcircuits

In the active subinterval $[t_0 : t_2]$, when the T1 is turned on, the inductor current i_L rises linearly in the range from $i_{L(min)}$

to $i_{L(max)}$. At instant t_2 the T_1 turns off. Accumulated energy of the inductor L is sufficient to discharge the C_{T2} and charge the C_{T1} capacitances in a resonant transition to enable ZVS turn on of the T_2. Next, in the passive subinterval $[t_3 : t_5]$ the inductor current i_L decreases linearly flowing through the load and the T_2. When i_L reaches predetermined negative threshold $i_{L(th)} > i_{L(min)}$, the T_2 turns off reinitiating resonant transition to recharge C_{T2} and discharge C_{T1} capacitances. After half of the resonant period, the ZVS conditions occur to turn on the T_1 and to restart the TCM operation.

C. TCM with capacitive snubber

At transistor T_1 turn off transients, an overvoltage can be induced due to rapidly decreasing current in stray inductances L_s of input power loop (Fig.1). In the following part, a snubber capacitor C_{sn} is applied to attenuate voltage spikes. Sizing of the snubber capacitor is based on energy balance equations. The energy E_{bf} before transistor T_1 turn off can be approximated by:

$$E_{bf} \approx \frac{I_{T1(max)}^2 L_s}{2} + \frac{2V_{T2(off)}^2 C_{T2(off)}}{3} + \frac{V_{T2(off)}^2 C_{sn}}{2} \quad (1)$$

where: $C_{T2(off)}$ - the voltage dependent drain-to-source capacitance $C_{DS}(V_{DS})$ of transistor T_2 in off state is obtained from the producer data-sheet capacitance characteristics $C_{DS} = C_{OSS} - C_{RSS}$ for $V_{DS} = V_i$. The energy stored in the drain-to-source capacitance C_{DS} at V_{DS} results from the following formula [19]:

$$E_{oss} = \frac{2C_{DS}(V_{DS})V_{DS}^2}{3} \quad (2)$$

and

$$I_{T1(max)} = \frac{V_i - V_o}{L}(t_2 - t_1) \quad (3)$$

The energy E_{af} after transistor T_1 turn off

$$E_{af} \approx \frac{2V_{T1(max)}^2 C_{T1(max)}}{3} + \frac{V_{T1(max)}^2 C_{sn}}{2} \quad (4)$$

where:
$V_{T1(max)}$ - the maximal value of overvoltage on T_1 and $C_{T1(max)}$ - the T_1 drain-to-source capacitance for $V_{T1(max)}$. Assuming the energy before transistor turn off equals to the energy after turned off:

$$E_{bf} = E_{af} \quad (5)$$

the capacitance of snubber capacitor C_{sn} is derived for acceptable $V_{T1(max)}$:

$$C_{sn} = \frac{3I_{T1(max)}^2 L_s + 4(C_{T2(off)}V_i^2 - C_{T1(max)}V_{T1(max)}^2)}{3(V_{T1(max)}^2 - V_i^2)} \quad (6)$$

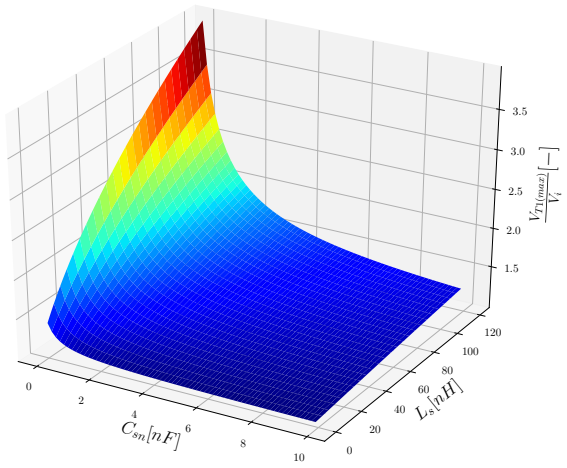

Fig. 6. Impact of snubber capacitor C_{sn} and input stray inductance L_s on voltage overshoot at the T1 turn off

III. Experimental Results

A. Test setup

The dc-dc buck converter shown in Fig. 1 was built using half-bridge connected two GaN HEMT in cascode structure of Transphorm (TPH3207WS: 650V/50A) with low pass LC filter, sized to the cut-off frequency f_c = 1630Hz. The converter was supplied from dc input voltage source V_i by the LISN Schaffner NNB 41. The resistive load R_l was set to dissipate 350W at the output voltage V_o = 55V.

Switching of GaN transistors was accomplished by the gate driver with two gate circuit branches as presented in Fig. 7. In this configuration, turn on and off time can be set individually using various values of R_1 and R_2 resistors respectively. Thus, switching performance is limited by resistor values, which determines the value of dv/dt existing in the converter. In the considered setup, a gate

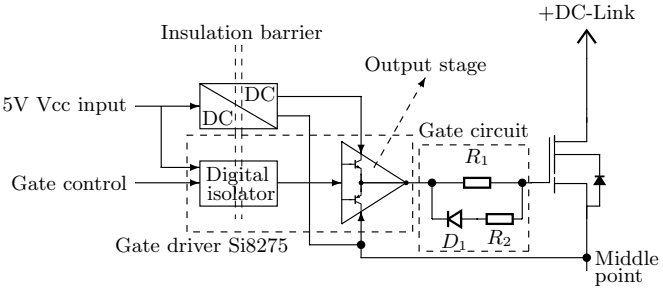

Fig. 7. Schematic of the gate driver

driver based on Si8275 IC was used to accomplish a signal insulation and the output stage of the driver. Moreover, two commercial DC-DC power supplies were used to provide independent powering of upper and lower switch. They create positive and negative voltages for driving each GaN device. Their stray capacitance is in the range of tens pF. Gate

This article has been accepted for publication in a future issue of this journal, but has not been fully edited. Content may change prior to final publication. Citation information: DOI 10.1109/JESTPE.2020.2987638, IEEE Journal of Emerging and Selected Topics in Power Electronics

circuits contained $R_{on} = 36\Omega$, $R_{off} = 10\Omega$ and provided voltages $V_{GS} = +8V/-2V$ for turn on and turn off switching.

The gating control pulses were generated using the STM32F407VG microcontroller. To obtain tight timing of gate signals, control program with three master-slave counters was configured to avoid delays deriving from internal interruptions in the microcontroller. In this way, the 40ns resolution for gate signal and dead times was obtained at the switching frequency f_s=80 kHz.
Using buck converter parameters from Table I in equation (6), an impact of snubber capacitor C_{sn} and input stray inductance L_s on $V_{T1(max)}/V_i$ voltage overshoot is calculated as in Fig. 6. This case study revealed increasing sensitivity of commutation transients for the input stray inductance L_s above 40nH. Minimization of L_s by careful circuit layout design is of primary importance. Otherwise, to attenuate turn off voltage overshoot, a snubber capacitor has to be applied. In the tested buck converter to limit turn off voltage overshoot to approximately 40% the C_{sn}=3.2nF was applied.

TABLE I
BUCK CONVERTER PARAMETERS IN TCM

Output power (P_o)	350W
Input voltage (V_i)	70V
Output voltage (V_o)	55V
Output current (I_o)	6.35A
Min. value of inductor current ($I_{L(min)}$)	–1.3A
Max. value of inductor current ($I_{L(max)}$)	15.2A
Input capacitor (C_i)	5.11μF
Input stray inductance (L_s)	114nH
Input stray resistance (R_s)	90$m\Omega$
Output capacitor (C)	1.1mF
Inductor (L)	8.7μH
Parasitic capacitance of T_2 in off state $C_{T2(off)}$	600pF

The switching strategies described above were compared in Fig. 8 by voltage waveforms across T_1 transistor. During DCM and TCM operation, at T_1 turn off significant overvoltage spikes had been recorded due to rapid decrease of current flowing through the stray inductances of input supply circuit. Only application of TCM with capacitive snubber attenuated overvoltage amplitudes, in accordance with analytical results of equation (6). In zero i_L current intervals of DCM operation, a typical resonant process between capacitances C_{T1}, C_{T2} and inductor L was evoked. In TCM strategy both transistors operated alternately with predetermined dead times for soft switching transitions.

For TCM+Csn Fig. 9 depicts, in larger time scale, current commutation from T_1 to T_2. The T_1 gate turn off initiated resonant charging of C_{T1} and discharging of C_{T2} with corresponding rate of change of transistor voltages: V_{T1} and V_{T2} that depended on load inductor current i_L. The LISN perturbation pulse was coherent with change of transistor voltages. After the recharging process had been completed the T_2 was turned on in ZVS conditions to conduct $i_L > 0$ as synchronous rectifier. To complete TCM sequences Fig. 10 presents load current

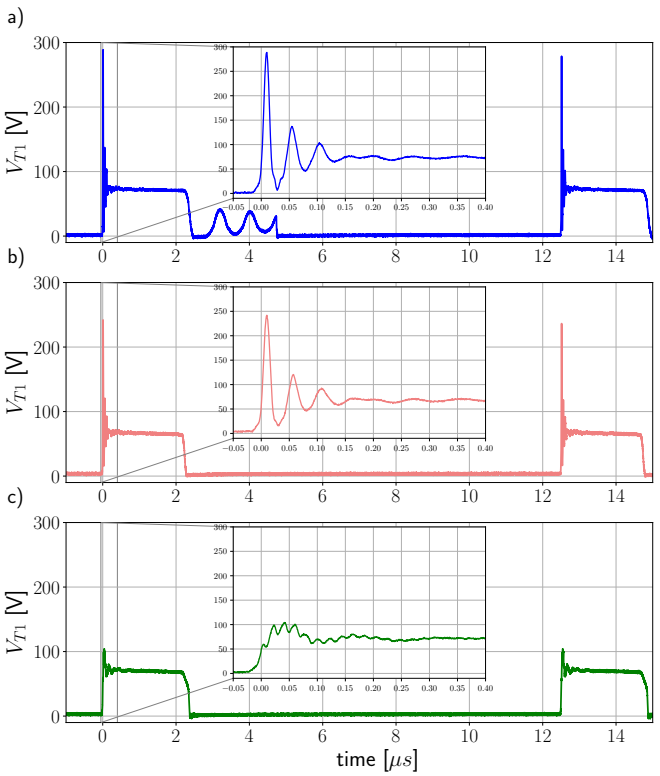

Fig. 8. Voltage waveforms across transistor T_1; a) DCM hard switching, b) TCM ZVS, c) TCM ZVS with snubber capacitors C_{sn}

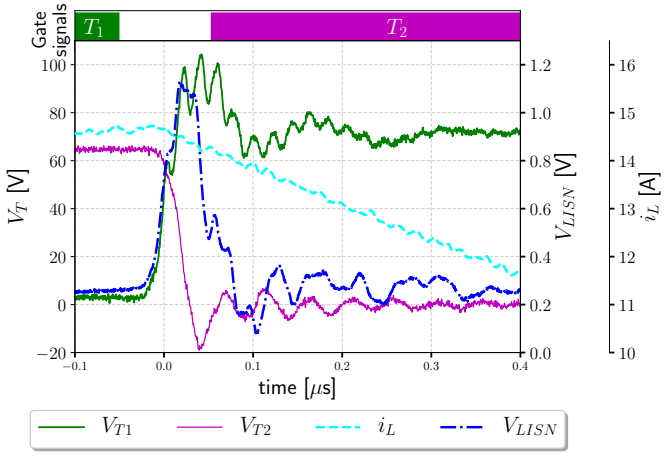

Fig. 9. ZVS of load current i_l from T_1 to T_2

commutation from T_2 to T_1. At predetermined $i_{L(th)} < 0$, the T_2 was turned off recharging nonlinear capacitances of both transistors. Due to near zero current transients, a lower rate of change of transistor voltages attenuated the LISN perturbation amplitude. At the end of recharging process, T_1 was turned on at ZVS. Comparative timing specification of TCM with and without capacitive snubber is presented in Table II. It is confirmed that the snubber impacts on extension of resonant transition periods (t_{d1}, t_{d2}) and dV_{T1}/dt turn off decrease.

This article has been accepted for publication in a future issue of this journal, but has not been fully edited. Content may change prior to final publication. Citation information: DOI 10.1109/JESTPE.2020.2987638, IEEE Journal of Emerging and Selected Topics in Power Electronics

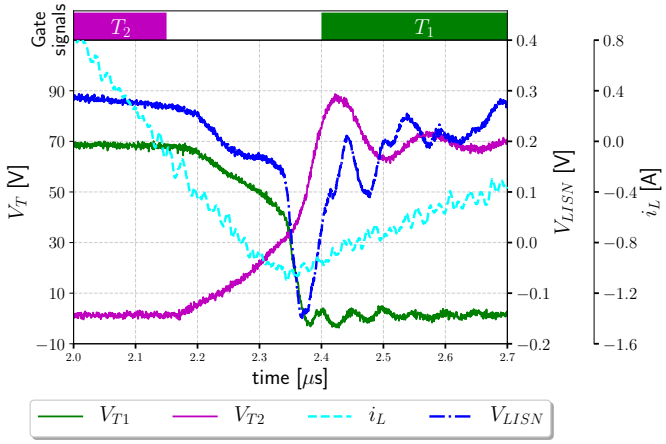

Fig. 10. ZVS of load current i_l from T_2 to T_1

TABLE II
TCM OPERATION WITHOUT AND WITH C_{sn}

	without C_{sn}	with C_{sn} ($3.2nF$)
T_1 on time ($t_{on-state(T_1)}$)	10.2μs	10.125μs
Dead time 1 (T_1 off and T_2 on) (t_{d1})	40ns	125ns
T_2 on time ($t_{on-state(T_2)}$)	2.05μs	2.0μs
Dead time 2 (T_2 off and T_1 on) (t_{d2})	210ns	250ns
Max. $\frac{dV}{dt}$ of V_{T1} during turn on	$1\frac{V}{ns}$	$1.3\frac{V}{ns}$
Max. $\frac{dV}{dt}$ of V_{T1} during turn off	$25.1\frac{V}{ns}$	$5.6\frac{V}{ns}$
V_{T1} falling time during turn on (t_f)	122ns	218ns
V_{T1} rising time during turn off (t_r)	30ns	48.5ns

B. Efficiency

Comparative experimental results of buck converter efficiency excluding the gate driving power are depicted in Fig. 11 for varying loads. An efficiency increase for ZVS TCM schemes over conventional DCM operation is evident. The highest (almost 1%) efficiency elevation was measured in the case of the TCM with capacitive snubber.

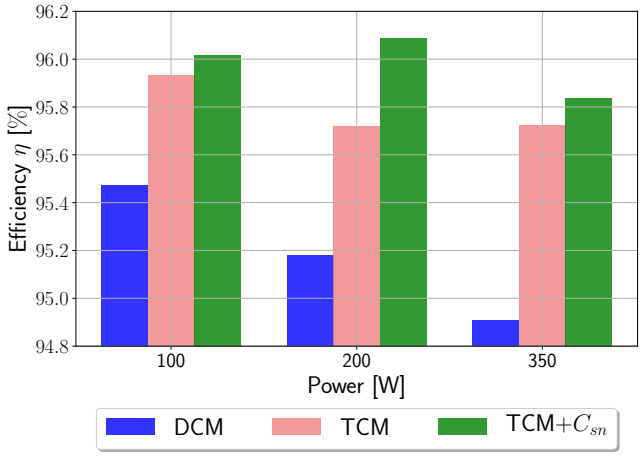

Fig. 11. Efficiency indexes

The results of analytical computation (as in [19]) of conductive and switching losses of the considered buck converter schemes are presented in Fig 12 for the rated output power.

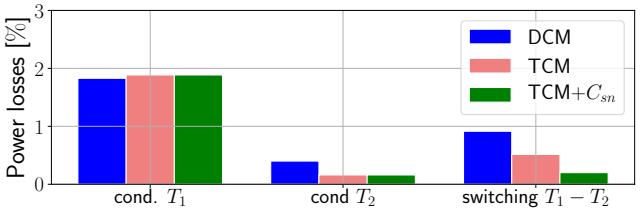

Fig. 12. Power loss distribution (P_o=350W)

The T_1 conduction loss is approximately constant due to comparable transistor current waveforms in the DCM and TCM operation. The T_2 conduction loss is decreased in the TCM because of synchronous rectification mode of operation. Main part of switching loss is caused by T_1 turn off. This is the energy lost in the resistance R_s of the charging path of C_{T1} capacitance and during the resonant turn off oscillations. In the DCM operation during turn on, the energy stored in the transistor capacitance is lost in the transistor on-resistance. During TCM operation, switching power loss is reduced due to resonant transition of the energy accumulated in transistor capacitances at the ZVS between T_1 and T_2.

C. EMI attenuation

In Figures 13-14 the spectra of common and differential modes are respectively presented for three switching strategies. The signals have been registered using LISN and separated offline for common and differential modes [20] using (7) and (8)

$$|V_{CM}| = \left|\frac{V_{LISN2} + V_{LISN1}}{2}\right| \tag{7}$$

$$|V_{DM}| = \left|\frac{V_{LISN2} - V_{LISN1}}{2}\right| \tag{8}$$

Both CM and DM EMI spectra indicate significant peaks of the switching frequency f_s harmonics, that are related to the triangular inductor current waveforms of converter operation.

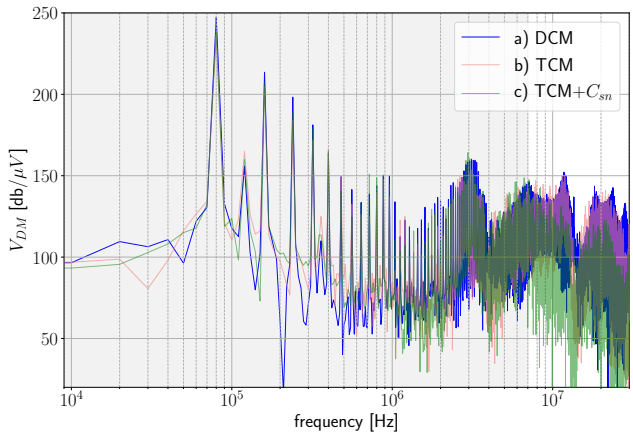

Fig. 13. EMI differential mode spectra

This article has been accepted for publication in a future issue of this journal, but has not been fully edited. Content may change prior to final publication. Citation information: DOI 10.1109/JESTPE.2020.2987638, IEEE Journal of Emerging and Selected Topics in Power Electronics

In order to analyze CM current loops during switching from T_1 to T_2, based on the buck converter test scheme from Fig 1, an equivalent circuit is derived as in Fig 16. The CM interference is propagated to the LISN RC branches in the loop containing parasitic capacitances between the heat-sink and the drain node $T_1 : C_{t-h}$, the drain node $T_2 : C_{m-h}$, the source node $T_2 : C_{b-h}$ and the ground C_{h-gnd} which affect the CM level. Since CM perturbation propagate by parasitic capacitances $C_{t-h}, C_{m-h}, C_{b-h}$ and C_{h-gnd}, the envelope spectra obtained for CM emission are higher than for the DM emission. In the range above 10MHz an impact of overvoltage peeks with ringing effects when T_1 turns off is observed (as was depicted by large scale voltage transients in Fig 15). To be noticed, emission levels are comparable for the DCM operation and for the TCM without snubber operation. But in the case of the TCM+C_{sn}, attenuation of the CM interference in the range starting from 7MHz reached almost -40dB at 20MHz.

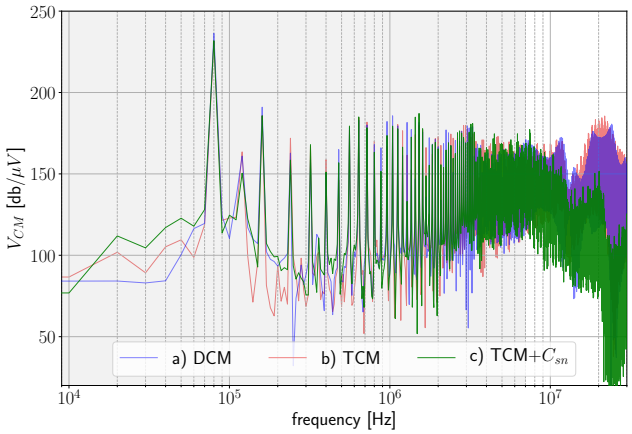

Fig. 14. EMI common mode spectra

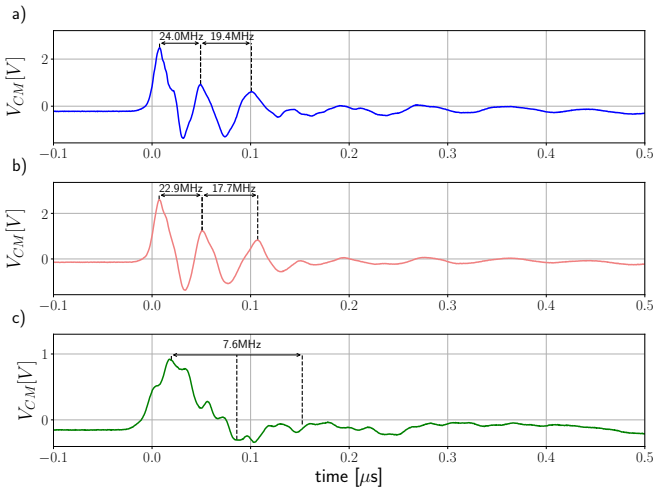

Fig. 15. CM voltage ripples during switching from T_1 to T_2 a) DCM b) TCM c) TCM+C_{sn}

The main components of parallel resonant circuit where the ringing interference is generated are the input stray inductance L_s, the nonlinear drain-to-source capacitance $C_{T1}(V_{DS})$ and the conductive path resistance R_s that are shunted by input filter capacitor C_i. Hence, the ringing frequency:

$$f_r \approx \frac{1}{2 * \pi * \sqrt{L_s * C_{T1}(V_{DS})}} \tag{9}$$

Since the nonlinear capacitance depends on drain-to-source voltage, the f_r varies in the range from 27 MHz for $C_{T1}(V_{T1(max)})$ to 17 MHz for $C_{T1}(V_i)$ (Figure 15). The parasitic capacitances to the heat-sink are also part of resonant loop, but their values are relatively much smaller than changes of $C_{T1}(V_{DS})$. Augmentation of C_{T1} by the snubber capacitance C_{sn} leads to attenuation of the voltage overshoot with frequency decrease of the ringing interference:

$$f_r \approx \frac{1}{2 * \pi * \sqrt{L_s * (C_{T1}(V_{DS}) + C_{sn})}} \tag{10}$$

The frequency f_r calculated using eq. 10 for parameters from Table I equals 7.64MHz.

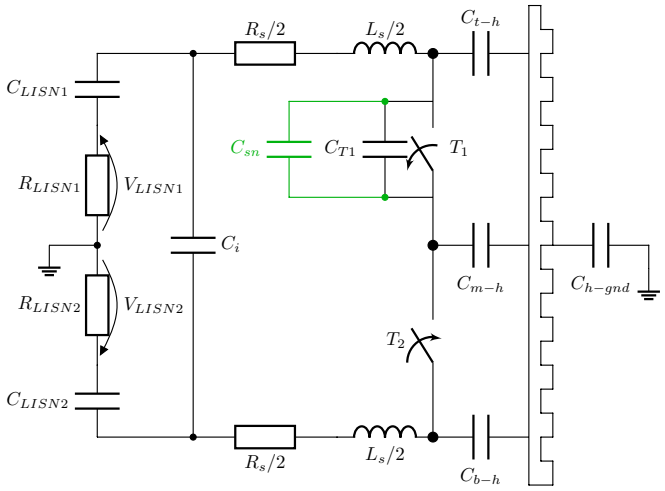

Fig. 16. Equivalent circuit of CM current loops during switching from T_1 to T_2

IV. Conclusion

In a GaN HEMTs based dc-dc buck converter the EMI conducted emissions were measured for discontinuous current mode and triangular current mode control strategies. Zero voltage switching that was achieved for the TCM operation revealed improvement of power conversion efficiency with the reference to the DCM operation. Implementation of capacitor snubbers across transistors for TCM operation slowed down transistor turn off process clamping voltage spikes. In consequence significant attenuation of common mode EMI emission with slight increase of power conversion efficiency were obtained. In order to fully exploit rapid switching ability of GaN HEMTs, recommendation of ZVS topology cannot be a sufficient condition but it must be accompanied by circuit design layout assuring extremely low parasitic inductances of commutation circuit loop.

REFERENCES

[1] R. Mitova, R. Ghosh, U. Mhaskar, D. Klikic, M. Wang, and A. Dentella, "Investigations of 600-V GaN HEMT and GaN diode for power converter applications," *IEEE Transactions on Power Electronics*, vol. 29, pp. 2441–2452, May 2014.

[2] D. Reusch and J. Strydom, "Evaluation of gallium nitride transistors in high frequency resonant and soft-switching DC–dc converters," *IEEE Transactions on Power Electronics*, vol. 30, pp. 5151–5158, Sept. 2015.

[3] X. Huang, Z. Liu, Q. Li, and F. C. Lee, "Evaluation and application of 600V GaN HEMT in cascode structure," in *Proc. Twenty-Eighth Annual IEEE Applied Power Electronics Conf. and Exposition (APEC)*, pp. 1279–1286, Mar. 2013.

[4] E. Gurpinar, Y. Yang, F. Iannuzzo, A. Castellazzi, and F. Blaabjerg, "Reliability-driven assessment of GaN HEMTs and Si IGBTs in 3L-ANPC PV inverters," *IEEE Journal of Emerging and Selected Topics in Power Electronics*, vol. 4, pp. 956–969, Sept. 2016.

[5] L. C. Murillo Carrasco and A. J. Forsyth, "Energy analysis and performance evaluation of GaN cascode switches in an inverter leg configuration," in *Proc. IEEE Applied Power Electronics Conf. and Exposition (APEC)*, pp. 2424–2431, Mar. 2015.

[6] E. Gurpinar, F. Iannuzzo, Y. Yang, A. Castellazzi, and F. Blaabjerg, "Design of low-inductance switching power cell for GaN HEMT based inverter," *IEEE Transactions on Industry Applications*, vol. 54, pp. 1592–1601, Mar. 2018.

[7] C. Fita, P. Jeannin, P. Lefranc, E. Clavel, and J. Delaine, "A novel 3D structure for synchronous buck converter based on nitride gallium transistors," in *Proc. IEEE Energy Conversion Congress and Exposition (ECCE)*, pp. 1–7, Sept. 2016.

[8] G. Regnat, P. Jeannin, D. Frey, J. Ewanchuk, S. V. Mollov, and J. Ferrieux, "Optimized power modules for silicon carbide mosfet," *IEEE Transactions on Industry Applications*, vol. 54, pp. 1634–1644, Mar. 2018.

[9] J. Schanen and P. Jeannin, "Integration solutions for clean and safe switching of high speed devices," in *Proc. CIPS 2018; 10th Int. Conf. Integrated Power Electronics Systems*, pp. 1–11, Mar. 2018.

[10] J. Biela, D. Hassler, J. Miniböck, and J. W. Kolar, "Optimal design of a 5kW/dm3/ 98.3% efficient tcm resonant transition single-phase pfc rectifier," in *Proc. Int. Power Electronics Conf. - ECCE ASIA -*, pp. 1709–1716, June 2010.

[11] X. Huang, F. C. Lee, Q. Li, and W. Du, "High-frequency high-efficiency GaN-based interleaved CRM bidirectional buck/boost converter with inverse coupled inductor," *IEEE Transactions on Power Electronics*, vol. 31, pp. 4343–4352, June 2016.

[12] D. M. Sable, F. C. Lee, and B. H. Cho, "A zero-voltage-switching bidirectional battery charger/discharger for the nasa eos satellite," in *Proc.] APEC '92 Seventh Annual Applied Power Electronics Conf. and Exposition [*, pp. 614–621, Feb. 1992.

[13] O. Knecht, D. Bortis, and J. W. Kolar, "ZVS modulation scheme for reduced complexity clamp-switch tcm DC–dc boost converter," *IEEE Transactions on Power Electronics*, vol. 33, pp. 4204–4214, May 2018.

[14] L. Middelstaedt, B. Strauss, A. Chupryn, and A. Lindemann, "Investigation of the root causes of electromagnetic noise of an interleaved DC-dc converter with GaN or si transistors and corresponding optimization strategies," *IEEE Journal of Emerging and Selected Topics in Power Electronics*, p. 1, 2019.

[15] X. Gong and J. A. Ferreira, "Investigation of conducted EMI in SiC JFET inverters using separated heat sinks," *IEEE Transactions on Industrial Electronics*, vol. 61, pp. 115–125, Jan. 2014.

[16] A. Dutta and S. S. Ang, "Electromagnetic interference simulations for wide-bandgap power electronic modules," *IEEE Journal of Emerging and Selected Topics in Power Electronics*, vol. 4, pp. 757–766, Sept. 2016.

[17] B. Sun, R. Burgos, and D. Boroyevich, "Common-mode EMI unterminated behavioral model of wide-bandgap-based power converters operating at high switching frequency," *IEEE Journal of Emerging and Selected Topics in Power Electronics*, vol. 7, pp. 2561–2570, Dec. 2019.

[18] M. Walczak, "Impact of inductor current ringing in dcm on output voltage of dc-dc buck power converters," *Archives of Electrical Engineering*, vol. 66, no. 2, pp. 313–323, 2017.

[19] M. K. Kazimierczuk, *Pulse-width modulated DC-DC power converters*. John Wiley & Sons, 2015.

[20] Yu-Kang Lo, Huang-Jen Chiu, and Tzu-Herng Song, "A software-based cm and dm measurement system for the conducted EMI," *IEEE Transactions on Industrial Electronics*, vol. 47, pp. 977–978, Aug. 2000.